scientific reports

OPEN

Research on the simulation methods and shock resistance performance of energy absorbing columns in rockburst roadway supports

Dong An, Jinying Fan, Yimin Song & Hailiang Xu✉

For the rockburst prevention issue of hydraulic supports in tunnel roadways, a structural design was introduced that adds energy-absorbing components to the hydraulic prop. This anti-shock hydraulic prop can improve the shock resistance of the support by absorbing energy through displacement. A solid-liquid coupling and static-dynamic coupling model for the anti-shock hydraulic prop was established using finite element and SPH particle methods. Impact tests were conducted on the energy-absorbing device and the shock-resistant prop with energy-absorbing columns. Optimization and adjustment of key simulation parameters were performed to achieve long-duration, high-precision simulations of energy-absorbing columns under shock loading in tunnel supports. The synergistic working mechanism between the energy-absorbing device and the hydraulic prop was revealed. The results show that the maximum displacement of the energy-absorbing column was reduced by 25% compared to the ordinary prop. The maximum displacement resistance was reduced by 18% compared to the ordinary prop. The total energy absorption was increased by 80% compared to the ordinary prop. It was found that the energy-absorbing device loaded on the energy-absorbing column could be fully crushed within 13 ms under the impact of a 10.5t hammer. The displacement speed reached 18.5 m/s, with variable stiffness and frequency.

Rockbursts commonly occur in tunnels and are one of the most severe dynamic hazards encountered in coal mining production[1–4]. Scholars have conducted extensive research in the field of rockburst prevention in tunnels, making valuable contributions to the understanding of tunnel surrounding rock failure mechanisms[5–8], support-rock interaction[9–11], and the development of tunnel support equipment[12,13]. Among them, tunnel hydraulic support plays a key role in rockburst prevention, and with the continuous advancement and refinement of rockburst occurrence mechanisms and theoretical research, the role of tunnel hydraulic supports in the initiation and failure process of rockbursts has gained increasing attention[12,14]. Installing energy-absorbing devices on traditional tunnel hydraulic support equipment has been a major advancement in rockburst prevention for mining supports in recent years. Research shows that energy-absorbing anti-shock supports can effectively enhance the shock resistance of tunnels[15]. The energy-absorbing anti-shock column is a key load-bearing component of tunnel rockburst prevention supports, and the shock resistance of the support is primarily achieved through the energy-absorbing anti-shock column[16,17]. Therefore, conducting research on the shock resistance of hydraulic support energy-absorbing columns in rockburst-prone tunnels is of significant theoretical and practical importance for the parameterization and structural design of energy-absorbing hydraulic supports.

Scholars have made many valuable research contributions in the fields of tunnel hydraulic support and energy-absorbing rockburst prevention, using theoretical derivations, field experiments, and numerical simulations. In terms of energy-absorbing device improvements, Hao[18] conducted experimental studies on the energy-absorbing devices and their filling materials in supports; Gao[19] optimized the structure of the energy-absorbing device and conducted experimental studies on its energy-absorbing performance. In terms of the

1School of Civil Engineering, North China University of Technology, Beijing, China. ✉email: xuhailiang@ncut.edu.cn

dynamic characteristics of hydraulic columns, Liu[20] performed numerical simulations of the dynamic response of hydraulic columns under impact loading using finite element and smooth particle hydrodynamics methods, Zhang[21] analyzed the performance of energy-absorbing anti-shock columns under ideal conditions using virtual simulation methods. However, existing research mainly focuses on the shock resistance of either the energy-absorbing device or the hydraulic column alone, with limited research on their coupled interaction, and the synergistic working mechanism between components requires further investigation. Simulations involve solid-liquid coupling between hydraulic emulsions and cylinder walls, as well as static-dynamic coupling between the column and energy-absorbing device, under high pressure and large deformations, traditional simulation methods cannot guarantee simulation accuracy, and their computational cost is high, making long-duration, high-efficiency simulations infeasible.

This paper uses a simulation method combining finite element analysis and SPH particle methods, and, by appropriately setting and adjusting relevant parameters, established a solid-fluid coupling model and fluid large deformation model for the anti-shock hydraulic prop. Impact tests were conducted on the energy-absorbing device and the anti-shock column, and key parameters in the simulations were optimized and adjusted, achieving long-duration, high-precision simulations of energy-absorbing anti-shock hydraulic columns. The shock process of the anti-shock hydraulic column was analyzed, and the synergistic working mechanism between the energy-absorbing device and hydraulic column was summarized. Based on the six design principles of anti-shock supports, the shock resistance of ordinary hydraulic columns and energy-absorbing anti-shock hydraulic columns was compared and quantified, which will further reveal the working mechanism of anti-shock hydraulic columns, enhance the shock resistance of supports, and provide references for the improvement of energy-absorbing hydraulic columns and anti-shock supports in future research, which has both theoretical and practical significance for improving rockburst mining efficiency and safety.

Shock-resistant hydraulic supports for rockburst roadways
Basic principles of support for rockburst roadway supports
When rockburst occurs, a large amount of energy is released, resulting in significant deformation, leading to instantaneous damage of several or even dozens of meters of roadway. Numerous engineering incidents have shown that ordinary hydraulic support structures have poor impact resistance, failing to provide effective support when rockburst inevitably occurs, as shown in Fig. 1.

Therefore, the support for rockburst roadways should adhere to the following principles[12,22]:

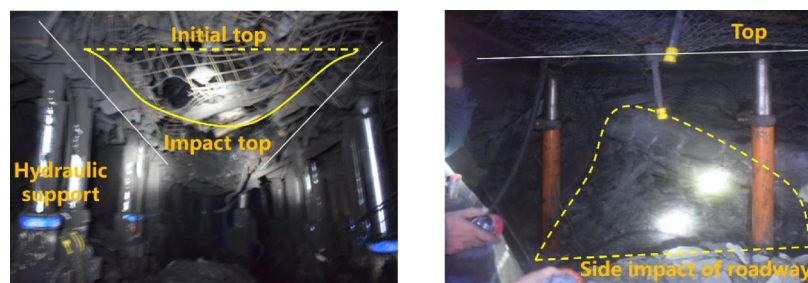*Principle of variable yield resistance*
Shock-resistant supports should have high support resistance to utilize this resistance against impact when rockburst initiates. Additionally, when the support resistance exceeds a certain threshold, it should yield at a relatively constant resistance until it stops, thereby continuously resisting and mitigating the damage caused by rockburst. Therefore, a special control device must be designed in the support to immediately activate and guide the support to deform when the impact load applied exceeds this threshold, allowing for a rapid cushioning process and ensuring the support remains intact while continuing to provide support.

Principle of variable yield displacement
Shock-resistant supports should be designed for variable yield displacement, meaning the yield displacement must coordinate with the deformation of the surrounding rock. When the support experiences impact loads from the surrounding rock that exceed a threshold, a special device in the support should immediately initiate deformation, enabling a rapid yield process for the entire support.

Principle of variable yield velocity
Shock-resistant supports should be designed for variable yield velocity. Under normal support conditions, they should slowly yield to relieve pressure when subjected to excessive quasi-static loads. However, once the impact load exceeds the support threshold, the yield components should initiate deformation at a higher speed to ensure a rapid response of the entire support.

(a) Roof Collapse in Roadways   (b) Sidewall Contraction

Fig. 1. Condition of roadway damage.

Principle of variable yield stiffness

The stiffness of the surrounding rock in the roadway is nonlinear; as roadway strain increases, stiffness gradually decreases, reaching zero during rockburst events. Shock-resistant supports should be designed with variable stiffness, possessing high structural stiffness to constrain the deformation of surrounding rock before rockburst occurs. After an unexpected impact from surrounding rock, the support should immediately initiate deformation, causing its structural stiffness to instantaneously become zero, coordinating with the stiffness of the surrounding rock to avoid overload damage due to excessive stiffness.

Principle of variable yield frequency

When the vibration frequency of the seismic source approaches the natural frequency of the support, it can lead to resonance, causing even minor seismic events to severely damage the support. Shock-resistant supports should possess variable natural frequency capabilities. Once a roadway impact occurs, the support should rapidly adjust its natural frequency to zero during the yield process to prevent resonance from vibration loads. When the surrounding rock impact ceases, the support should resume its supporting function, establishing a new natural frequency.

Principle of variable yield energy

Shock-resistant supports must have the capability to absorb energy during yielding, meaning that under sudden large impacts from surrounding rock, the impact energy can be absorbed by specially designed devices within the support, while the support yields to a certain extent. The amplitude of yielding and the amount of energy absorbed vary with the impact energy. The energy absorption process of the support rapidly dissipates the impact energy from the surrounding rock, thereby protecting the overall structure of the support from damage and ensuring the stability and safety of the entire roadway support system.

Structural design of energy-absorbing shock-resistant hydraulic supports

There are various types of hydraulic supports for roadways, with the main load-bearing structures typically comprising the top beam, base, and corresponding hydraulic columns. The top beam and base primarily serve to transfer forces, constrain, and guide, making it difficult to implement yield energy absorption designs, which offer limited improvement in shock resistance. In accordance with the basic principles of support for rockburst roadways, our research team's approach is to add a cylindrical sleeve to the bottom of the hydraulic column, within which a yield energy-absorbing component is placed, forming an energy-absorbing shock-resistant hydraulic column. Various structures of hydraulic supports with differing shock resistance, developed as a result, are shown in Fig. 2. The designs meet the requirements of the standard GB25974.2-2010 and have been implemented in rockburst mines such as Gengcun Coal Mine, Longjiabao Coal Mine, and Laohutai in Liaoning, China.

A simplified structural model of the FCZ1650/25/42 energy-absorbing hydraulic column loaded by a unit-type energy-absorbing hydraulic support is shown in Fig. 3. It consists of four parts: hydraulic piston, high-pressure cylinder, low-pressure cylinder, and energy-absorbing sleeve, with the cylinder filled with emulsified liquid. The energy-absorbing sleeve houses the yield energy-absorbing device, and the core technical parameters of the column and the energy-absorbing device are listed in Table 1. The energy-absorbing device is a thin-walled metallic cylinder with a special geometric shape, as illustrated in Fig. 4. The energy-absorbing device is designed with initial folds that ensure it collapses in a predetermined direction under impact loads, while also absorbing energy to achieve the effect of yield energy absorption for shock resistance[23,24].

The energy-absorbing shock-resistant hydraulic column has a specific activation load. When the overall load on the shock-resistant column is below the working resistance, the energy-absorbing device does not deform until the activation load is reached, providing stable support to constrain the deformation of the surrounding
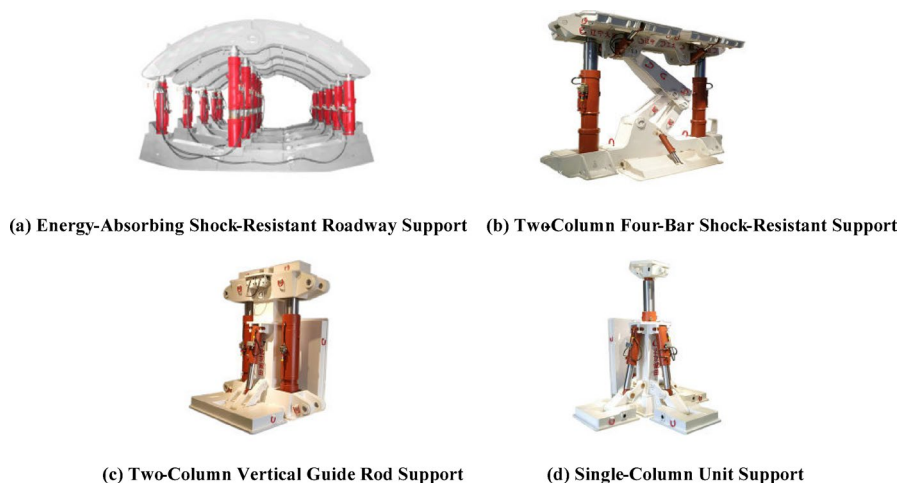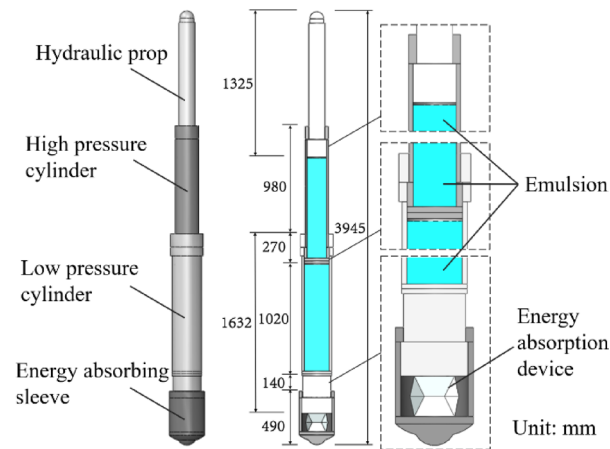

(a) Energy-Absorbing Shock-Resistant Roadway Support   **(b) Two-Column Four-Bar Shock-Resistant Support**

(c) Two-Column Vertical Guide Rod Support   **(d) Single-Column Unit Support**

Fig. 2. Energy-absorbing shock-resistant hydraulic support types.

Fig. 3. Energy-absorbing shock-resistant hydraulic column model.

Hydraulic column	Technical parameters
Cylinder inner diameter (mm)	Φ230/Φ180
Cylinder wall thickness (mm)	21.5/17.5
Initial support force (MPa/kN)	31.5/1309
Working resistance (MPa/kN)	39.5/1650
Energy-absorbing device	**Technical parameters**
Yield resistance (kN)	3300
Material strength (MPa)	890
Wall thickness (mm)	8
Design yield displacement (mm)	120

Table 1. Parameters of energy-absorbing shock-resistant hydraulic supports.
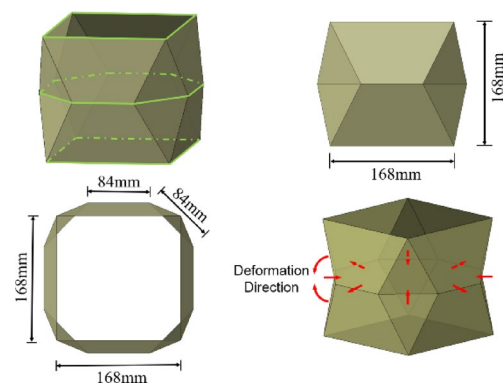
Fig. 4. Dimensions of the energy-absorbing device.

rock. During a severe impact on the surrounding rock, the energy-absorbing device rapidly absorbs energy and yields, allowing the hydraulic cylinder to displace under guidance, thus protecting all parts of the column from damage. After the impact, the energy-absorbing shock-resistant column can continue to provide effective support for the roadway while preventing secondary disasters.
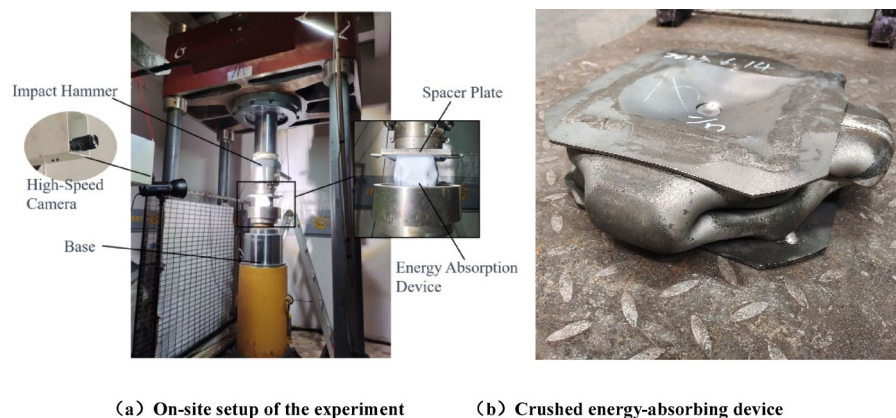
（a）On-site setup of the experiment　　　（b）Crushed energy-absorbing device

Fig. 5. Crushing test of the energy-absorbing device.

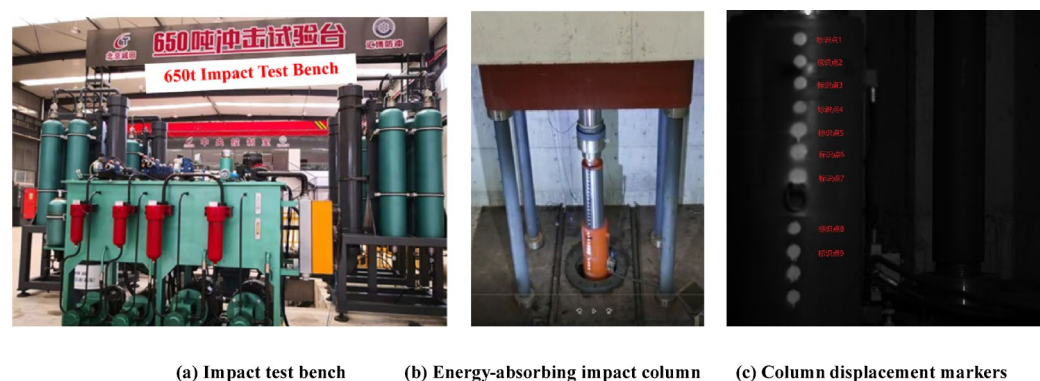(a) Impact test bench　　　(b) Energy-absorbing impact column　　　(c) Column displacement markers

Fig. 6. Photos of the on-site experimental environment.

Energy-absorbing shock-resistant hydraulic column testing and simulation parameter optimization
Field testing
Energy-absorbing device testing
Field experiments were conducted on the compressed energy-absorbing device using a shock testing platform, with the environmental setup shown in Fig. 5(a). The energy-absorbing device was placed on the impact base, with a pad placed on top to ensure uniform pressure on the specimen as much as possible. Sensors were used to record the force and displacement data of the energy-absorbing device during the crushing process, while a high-speed camera captured the crushing process of the device. The crushed energy-absorbing device is shown in Fig. 5(b).

Column impact testing
A field test was conducted on the FCZ1650/25/42 energy-absorbing hydraulic column loaded with an energy-absorbing device using a 650-ton pneumatic impact testing platform, with the base of the column fixed to the platform for impact loading. A high-speed camera was used to capture the displacement marker data on the cylinder wall of the column during the impact process, allowing for the plotting of the displacement curve of the column under impact load. Figure 6 (a) shows the pneumatic system of the testing platform, Fig. 6 (b) shows the energy-absorbing shock-resistant column mounted on the platform, and Fig. 6 (c) shows the displacement markers captured by the high-speed camera.

Finite element simulation parameter adjustment
Basic parameter settings
The FCZ1650/25/42 energy-absorbing hydraulic column is a double-telescopic column. Minor components like the pressure relief valve are neglected, and models for the high-pressure cylinder, low-pressure cylinder, hydraulic piston, energy-absorbing sleeve, and energy-absorbing device are created and assembled separately. Based on the materials used in actual engineering, the yield strength of the cylinder steel is set to 835 MPa, with an elastic modulus of 206 GPa and a Poisson's ratio of 0.3, using C3D8R elements. A fixed constraint is applied at the bottom of the energy-absorbing sleeve, while horizontal displacement is restricted at the top of the hydraulic piston, with no constraints at other locations. The energy-absorbing device is 168 mm high and only 8 mm thick,

Kernel	Quadratic	Cubic	Quintic
Error rate	4.4%	2.6%	2.2%

Table 2. Error for different "kernel" values.

PPT	1	2	3	4
Error rate	2.3%	1.6%	1.4%	1.2%

Table 3. Error for different "PPT" values.
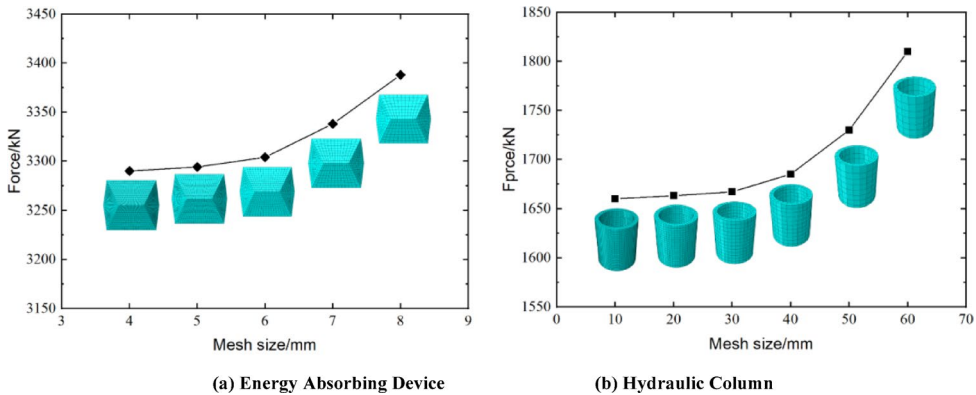

(a) Energy Absorbing Device   (b) Hydraulic Column

Fig. 7. Grid division of energy absorbing device and hydraulic column.

a difference of more than 20 times, classifying it as a thin-walled structure. It is modeled using shell elements, with the yield strength of high-strength steel set to 890 MPa, an elastic modulus of 206 GPa, and a Poisson's ratio of 0.26, using S4R elements, and placed inside the energy-absorbing sleeve.

Key parameter optimization

Emulsified liquid SPH particle parameters   First, the basic properties of the emulsified liquid are defined, with the US-UP fluid state equation specified, setting c0 = 1400 m/s, s = 0, Gamma = 0, and a density of 1.08 t/m³. After establishing the solid model, the "Convert to Particles" option is checked in the element control properties interface of ABAQUS software to enable the meshless particle simulation of the emulsified liquid (SPH). The key settings "Kernel" (which affects the calculation accuracy and depth of the software) and "PPT" (which influences the number of particles after mesh conversion) are varied, and the calculation result errors are shown in Tables 2 and 3, where the simulation error is the difference between the theoretical liquid pressure of the hydraulic column during operation and the simulated result. Considering calculation accuracy and resource consumption, cubic spline interpolation is chosen, with PPT set to 2, ensuring that the error remains within 3% while maintaining a high simulation calculation speed.

Element mesh size   The denser the mesh division of the model, the higher the accuracy of the calculation results, but this also leads to increased resource consumption. For small-sized, critically stressed components, a finer mesh should be used, while larger, non-critical components can have a coarser mesh to reduce the number of elements. The calculation results of the working resistance of the cylinder body and energy-absorbing device of the FCZ1650/25/42 hydraulic column under different mesh sizes are shown in Fig. 7. The mesh size for the cylinder body is set to 30 and for the energy-absorbing device to 6, resulting in a total of 14,200 elements for the anti-collision column, with a comprehensive error rate of 3.2%.

Friction coefficient   The crushing deformation process of the energy-absorbing device is significantly influenced by friction, which alters the crushing resistance curve of the device and subsequently affects the deformation process of the energy-absorbing anti-shock column. Generally, the larger the friction coefficient, the higher the peak crushing resistance of the energy-absorbing device. Based on the measurement results from field tests and related research data on energy-absorbing devices by scholars [25,26], The error analysis for different friction coefficient values is shown in Table 4. The friction coefficient between the energy-absorbing device and the energy-absorbing sleeve is ultimately set to 0.3, and friction at the contact surface between the hydraulic cylinder and hydraulic emulsion is neglected. The overall finite element mesh model of the anti-shock column is shown in Fig. 8.

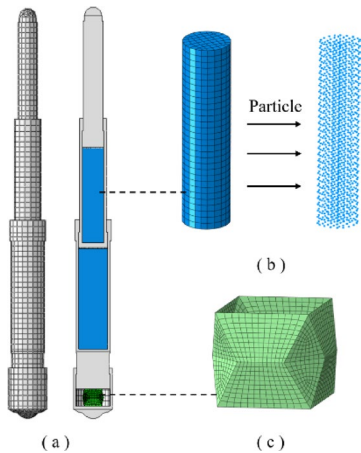| Testing methods and values	Experiment (0.31)	Simulation (0.2)	Simulation (0.25)	Simulation (0.3)	Simulation (0.35)
Max force of the device	1760	1540	1605	1788	2014
Reaction force error value	0	12.5%	8.8%	1.2%	14.4%

Table 4. Errors under different friction coefficient values.

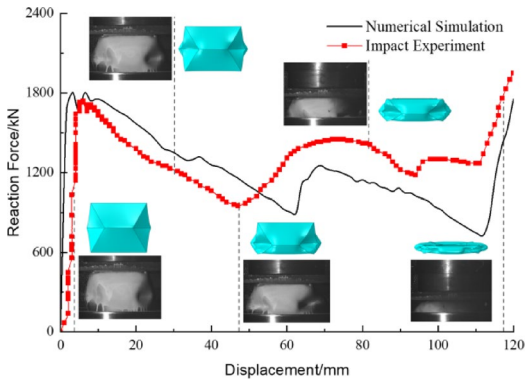**Fig. 8**. Simulation method for energy absorbing anti-impact column.

Fig. 9. Force-displacement curve of the energy absorbing device.

Optimization results
The force-displacement curve during the crushing process of the energy-absorbing device is shown in Fig. 9. It can be observed that the optimized simulation results align well with the experimental data. After the impact begins, the reaction force of the energy-absorbing device immediately reaches its maximum value, with a maximum reaction force of 180 kN in the experiment and 174 kN in the simulation, resulting in a discrepancy of less than 3%. The reaction force curve of the energy-absorbing device during the crushing process exhibits a "W" shape, providing a relatively stable load-bearing capacity.

The displacement of the cylinder wall marker points in the anti-collision column simulation is compared with the results from the field experiment, as shown in Fig. 10, where time zero represents the moment the impact begins. The optimized finite element simulation results match well with the experimental results, showing that the low-pressure cylinder segment of the hydraulic column begins to deform approximately 10 ms after the impact starts, with the deformation rate gradually increasing. The deformation rate slows down and eventually stabilizes about 38 ms after the impact. Over a period of 28 ms, the displacement of the experimental column increased from 3.9 mm to 98.3 mm, a total increase of 94.4 mm; meanwhile, the simulated column displacement increased from 9.2 mm to 107.9 mm, a total increase of 98.7 mm, with an error rate of 4.4%.

Impact resistance of the energy-absorbing hydraulic column
To further investigate the impact resistance of the energy-absorbing hydraulic support column, the author conducted a numerical simulation of this model under heavy hammer impact. A concentrated force equivalent
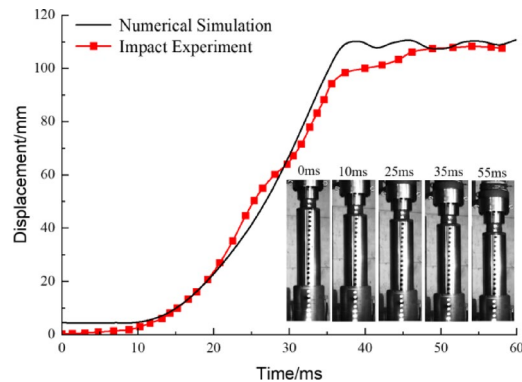
Fig. 10. Comparison of field experiment and simulation results.
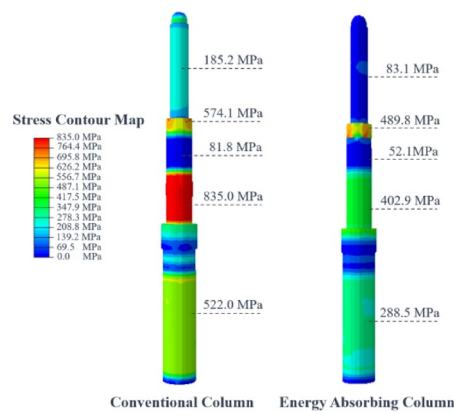

Fig. 11. Stress cloud map of cylinder wall.

to 0.6 times the working resistance was gradually applied to the hydraulic piston at the top of the column to represent the initial supporting force of the hydraulic column, after which the heavy hammer impact was released once the system stabilized. According to the design specifications, this model of the impact-resistant column can withstand a strong impact from a 7 t hammer at a speed of 8 m/s. With an interval coefficient of 0.5, 4.5 t, 7 t, and 10.5 t hammers were used to impact both the ordinary hydraulic column and the energy-absorbing hydraulic column at a speed of 8 m/s[22].

Yield resistance

The stress on the column wall can reflect the level of support resistance. Taking the 7 t hammer impact as an example, the stress cloud diagrams at the peak stress moments for both columns are shown in Fig. 11.

The ordinary hydraulic column failed under impact when the wall stress reached the yield strength of 835 MPa, while the maximum wall stress of the energy-absorbing column was only 402.9 MPa, indicating a significant anti-impact effect. The changes in support resistance over time for both columns under a 7 t hammer impact are shown in Fig. 12. After 28 ms of the impact, the support resistance of the energy-absorbing column rose to about 3700 kN before declining, and it rebounded at 39 ms post-impact. The ordinary column was destroyed 26 ms after the impact, and its support resistance did not increase further, beginning to decline at 43 ms post-impact. The maximum values of the column support resistance under different hammer impacts are shown in Table 5.

Yield displacement

Taking the 7 t hammer impact as an example, the displacement time histories for both hydraulic columns are shown in Fig. 13, where time 0 marks the beginning of the impact. The ordinary hydraulic column reaches a maximum displacement of 260 mm at 39 ms post-impact. In contrast, the energy-absorbing hydraulic column's absorbing device initiates deformation and quickly yields at 23 ms post-impact, reducing the column's displacement from 200 mm to 123 mm. At 39 ms, the absorbing device is completely crushed, and after its failure, the column's displacement rebounds, resulting in a second peak displacement. The maximum displacements of both columns under different hammer impacts are shown in Table 6. Under impacts from 4.5 t, 7 t, and 10.5 t hammers, the displacement of the energy-absorbing column is reduced by 16%, 23%, and 30%, respectively, compared to the ordinary column.
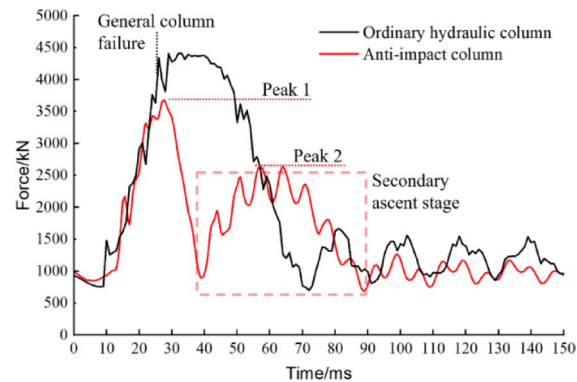
Fig. 12. Time history curve of column support resistance.

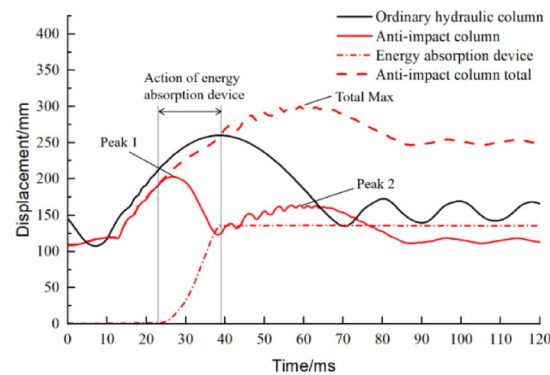| Hammer weight	4.5t	7t	10.5t
Ordinary column	4124 kN	4409 kN	4409 kN
Energy-absorbing column	3575 kN	3643 kN	3928 kN

Table 5. Maximum values of column support resistance.
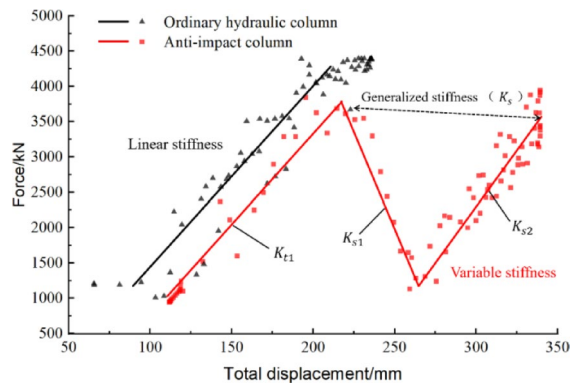

**Fig. 13**. Column displacement time history curve.

Hammer weight	4.5 t	7 t	10.5 t
Ordinary column	222 mm	261 mm	291 mm
Energy-absorbing column	187 mm	199 mm	204 mm
Energy-absorbing device	101 mm	135 mm	136 mm

Table 6. Maximum column displacement.

Yield velocity

The maximum yield velocities of the columns under impact loads are shown in Table 7. The energy-absorbing hydraulic column exhibits the fastest yield velocity during elastic deformation and has recoverability, making it suitable for frequent small seismic impacts from surrounding rock. Under large seismic impacts, the yield velocity during plastic deformation of the absorbing device is slightly lower. Ideally, it should have low viscosity and high plasticity. When achieving ideal plasticity, it also exhibits the fastest deformation velocity, allowing for rapid yielding of the support and meeting the velocity requirements for impact protection. As shown in Table 5, under strong impacts, the crushing speed of the energy-absorbing device is faster, and the duration of deformation is shorter. Due to the combined effects of column rebound and external loading, the yield velocity of the absorbing device exceeds the impact speed of the hammer, allowing it to respond instantaneously to high-speed impacts from the surrounding rock.

Hammer weight	4.5 t	7 t	10.5 t
Maximum speed of hydraulic column	7.89 m/s	8.12 m/s	8.33 m/s
Maximum speed of energy-absorbing device	11.1 m/s	13.4 m/s	18.5 m/s
Crushing duration of energy-absorbing device	18 ms	15 ms	13 ms

Table 7. Column yielding velocity.

Fig. 14. Column displacement and bracing resistance.

(a) Base Reaction Force Time History   (b) Reaction Force Spectrum
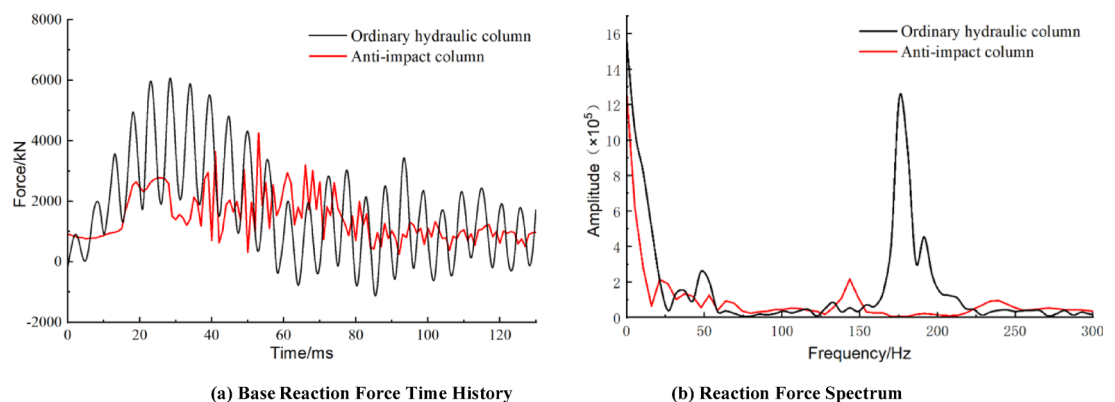
Fig. 15. Base reaction force time history and spectrum of the column.

Yield stiffness

The ordinary hydraulic column possesses only elastic stiffness. The energy-absorbing device features variable stiffness, allowing for the adjustment of the overall structural stiffness of the energy-absorbing hydraulic column. The displacement-support resistance curves for both types of columns under impact loads are shown in Fig. 14. The energy-absorbing hydraulic column exhibits elastic stiffness before and after the deformation of the energy-absorbing device. During the crushing of the energy-absorbing device, it demonstrates plastic stiffness. The elastic stiffness values are $Kt1 = 3.08 \times 10^7$ N/m and $Kt2 = 3.49 \times 10^7$ N/m, with the plastic stiffness being $Ks = -4.31 \times 10^7$ N/m, where the plastic stiffness is negative. The elastic yielding stiffness provides reasonable deformation constraint capability and elastic buffering effect to the support against the surrounding rock, defending against frequent impacts from minor seismic events. The plastic yielding stiffness can adjust the structural stiffness of the support after overload, quickly reducing the peak impact force from the surrounding rock, thus meeting the stiffness requirements for impact protection.

Yield frequency

When the vibration frequency of the surrounding rock is close to the natural frequency of the support, resonance occurs with the support, at this point, even small seismic events can cause severe damage to the support. The ideal frequency of the energy-absorbing device during the plastic deformation phase is zero, which allows for an instantaneous change in the natural frequency of the column during overload. A fast Fourier transform (FFT) of the foundation reaction under impact loads on both types of columns was performed with a 7t hammer impact, The column reaction force and the reaction force spectrum are shown in Fig. 15. The energy-absorbing
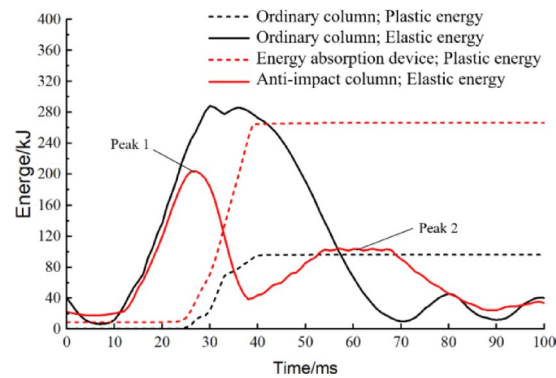
Fig. 16. Column energy time history.

Hammer weight	4.5 t	7 t	10.5 t
Elastic energy of energy-absorbing column	198 kJ	204 kJ	223 kJ
Plastic energy of energy-absorbing device	112 kJ	266 kJ	272 kJ
Elastic energy of ordinary column	247 kJ	279 kJ	280 kJ
Plastic energy of ordinary column	0	96 kJ	210 kJ

Table 8. Yielding energy of the column.

hydraulic column has a frequency of zero under impact deformation, which can completely prevent resonance of the column and support under the impact and vibration of the surrounding rock.

Yield energy

The hydraulic column should have the ability to store and absorb energy, ensuring that the support structure remains undamaged. The hydraulic cylinder undergoes elastic deformation to store elastic energy, while the energy-absorbing device undergoes plastic deformation to absorb energy. The energy time histories of both types of columns under a 7 t hammer impact are shown in Fig. 16. The elastic energy of the ordinary hydraulic column's cylinder reaches 280 kJ and then stops increasing, and begins to undergo plastic deformation, ultimately reaching a plastic deformation energy of 96 kJ; the peak elastic energy of the energy-absorbing hydraulic column's cylinder is 204 kJ, which is a 27% reduction compared to the ordinary column, while the plastic energy absorption of the energy-absorbing device is 266 kJ.

The yield energy of both columns under different hammer impacts is shown in Table 8. For the ordinary hydraulic column, under the impacts of 7t and 10.5t hammers, the cylinder reaches its maximum elastic energy before undergoing plastic deformation; For the energy-absorbing hydraulic column, the maximum elastic energy of the column is around 200 kJ, and the cylinder does not undergo plastic deformation.

Anti-scour process of the column

The anti-shock response of the energy-absorbing hydraulic column under a 7t hammer impact is shown in Fig. 17. Based on the above research, the collaborative operation between the energy-absorbing device and the hydraulic column can be divided into four stages: The first stage is the column pressure-bearing stage, where the column displacement starts to increase at 10 ms, but the energy-absorbing device has not yet started to deform. The second stage is the energy-absorbing device action stage, where the device begins to crush at 25 ms, rapidly absorbing energy, and stops deforming after reaching the design displacement at 39 ms. The third stage is the resistance recovery stage, where from 44 ms to 61 ms, after the energy-absorbing device fails, the hydraulic system continues to resist the impact, and the column displacement increases again. The fourth stage is the pressure relief stage, where the impact hammer's kinetic energy drops to zero at 61 ms, and the column's elastic energy remains for about 12 ms before gradually decreasing.

It is noteworthy that studies using simplified models generally assume that the energy-absorbing device provides a stable resistance during deformation, leading to the conclusion that the hydraulic system of the column will remain in a high-pressure state during the crushing process of the energy-absorbing device[21]. However, as the resistance of the energy-absorbing device fluctuates and decreases to some extent after deformation begins, the data in Fig. 17 show that the load borne by the column rapidly decreases once the energy-absorbing device starts to deform. After the energy-absorbing device completely fails, the load increases again. This will provide new insights for the research and development improvements of the energy-absorbing hydraulic column.
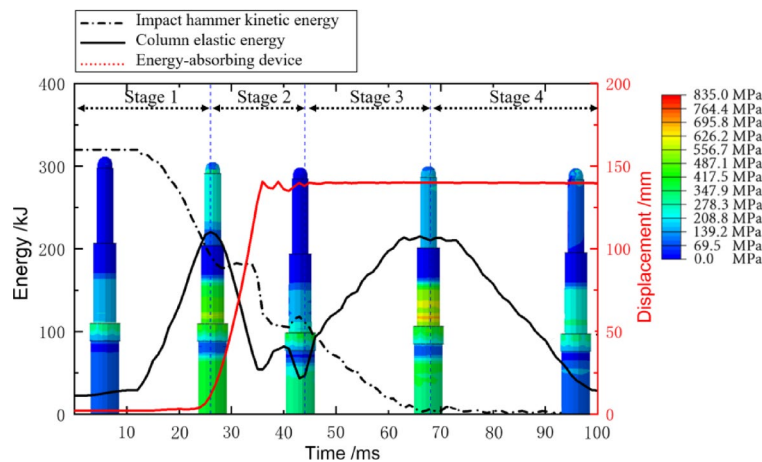
Fig. 17. Column anti-impact response stage.

Conclusion

(1) Summarized the six principles of tunnel anti-shock support design, analyzed the hydraulic support anti-shock design concept, and introduced a type of energy-absorbing anti-shock hydraulic column, which significantly improves the column's anti-shock performance by adding an energy-absorbing sleeve and loading an energy-absorbing device at the base of the column.

(2) Used finite element and SPH simulation methods to implement the finite element simulation of the energy-absorbing anti-shock hydraulic column under impact loads. Impact tests of the energy-absorbing device and anti-shock hydraulic column were conducted using an impact testing machine. Based on the experimental results, three key parameters—particleization settings, unit mesh size, and friction coefficient—were optimized, and the final simulation results had a deviation of less than 5% from the experimental data, verifying the feasibility and accuracy of the simulation method.

(3) Based on the six principles of anti-shock support design, the anti-shock performance of the hydraulic support column was discussed from six aspects: column displacement resistance, displacement, velocity, stiffness, frequency, and energy. The improvements of the energy-absorbing hydraulic column compared to the ordinary hydraulic column were quantified. The results show that: the maximum displacement resistance of the energy-absorbing column is 18% lower than that of the ordinary column; the maximum compression displacement of the energy-absorbing column is reduced by 29.8%; the maximum displacement speed of the energy-absorbing device under a 7t impact is 8.12 m/s; the overall stiffness of the energy-absorbing column is variable during displacement anti-shock; the inherent frequency of the energy-absorbing column during displacement anti-shock is 0; and the overall energy absorption of the energy-absorbing column is 75% higher than that of the ordinary column, making it less prone to plastic failure under the same impact.

(4) Summarized that the anti-shock response process of the energy-absorbing hydraulic column can be divided into four stages: elastic pressure-bearing stage, energy-absorbing device action stage, resistance recovery stage, and pressure relief stage, and revealed the collaborative working mechanism between the two. This provides a reference for further research and improvements in tunnel anti-shock hydraulic support columns.

Data availability

All data, models, or code that support the findings of this study are available from the corresponding author upon reasonable request.

References

1. Dou, L. M., Tian, X. Y., Cao, A. Y. & Gong, S. Y. Present situation and problems of coal mine rock burst prevention and control in China. *J. China Coal Soc.* **47** (01), 152–171 (2022).
2. Farhadian, H. A new empirical chart for rockburst analysis in tunnelling: tunnel rockburst classification (TRC). *Int. J. Min. Sci. Technol.* **31** (4), 603–610 (2021).
3. Pan, Y. S., Lu, X. F. & Li, Z. H. The model of energy-absorbing coupling support and its application in rock burst roadway. *J. Min. Saf. Eng.* **28** (01), 6–10 (2011).
4. Xu, L. M., Lu, K. X., Pan, Y. S. & Qin, Z. J. Study on rock burst characteristics of coal mine roadway in China. *J. Energy Sources Part A Recov. Util. Environ. Eff.* **44** (2), 3016–3035 (2022).
5. Pan, Y. S., Qi, Q. X., Wang, A. W., Xiao, Y. H. & Chen, J. Q. Theory and technology of three levels support in bump-prone roadway. *J. China Coal Soc.* **45** (05), 1585–1594 (2020).
6. Yang, Y. Z., Wang, Y. J. & Wu, K. Numerical study on dynamic fracture and energy transformation characteristics of rock unloading failure under identical energy stored levels. *Int. J. Geomech.* **23**(12) (2023).

7. Yang, Y. Z. & Zhang, Z. N. Dynamic fracturing process of fissured rock under abrupt unloading condition: A numerical study. *Engi. Fract. Mech.*, 231 (2020).
8. Yang, Y. Z., Shao, Z. S., Wu, K. & Wang, Y. J. A plastic Stillinger-Weber potential-based discretized virtual internal bond approach for modeling soft rock fracture and its application in tunnel failure. *Eng. Fract. Mech.*, 301 (2024).
9. Carranza-Torres, C. & Diederichs, M. Mechanical analysis of circular liners with particular reference to composite supports. For example, liners consisting of shotcrete and steel sets. *Tunn. Undergr. Space Technol.* **24** (5), 506–532 (2009).
10. Oreste, P. P. Analysis of structural interaction in tunnels using the covergence–confinement approach. *Tunn. Undergr. Space Technol.* **18** (4), 347–363 (2013).
11. Mitelman, A. & Elmo, D. Analysis of tunnel-support interaction using an equivalent boundary beam. *Tunn. Undergr. Space Technol.* **84**, 219–226 (2019).
12. Pan, Y. S., Xiao, Y. H. & Li, G. Z. Roadway hydraulic support for rockburst prevention in coal mine and its application. *J. China Coal Soc.* **45** (01), 90–99 (2020).
13. Wang, G. F. & Pan, Y. H. Shield-roof adaptability evaluation method based on coupling of parameters between shield and roof strata. *J. China Coal Soc.* **41** (6), 1348–1353 (2016).
14. Xu, L. M., Lu, K. X., Pan, Y. S. & Qin, Z. J. Research on the relationship between coal burst tendency and rockburst risk of coal seam. *J. Energy Sources Part A Recov. Util. Environ. Effects.* (2020).
15. Pan, Y. S. Disturbance response instability theory of rockburst in coal mine. *J. China Coal Soc.* **43** (8), 2091–2098 (2018).
16. An, D. et al. Study of the factors influencing load displacement curve of energy absorbing device by area division simulation. *Sci. Rep.* **12**(1), (2022).
17. Ma, X., Pan, Y. S., Zhang, J. Z. & Xiao, Y. H. Design and performance research on core energy absorption component of anti-impact support. *J. China Coal Soc.* **43** (04), 1171–1178 (2018).
18. Hao, Z. Y., Liu, Y. Q. & Pan, Y. S. Experimental study on filling material of mining buffer energy absorption device. *J. Min. Saf. Eng.* **35** (03), 620–628 (2018).
19. Gao, Y. X., Tan, M. & Xie, M. Application of hydraulic support for roadway advance support in Yuejin coal mine. *J. Coal Sci. Technol.* **45** (09), 3325–3332 (2020).
20. Liu, X. K., Zhao, Z. H. & Zhao, R. Study on dynamic features of leg applied to hydraulic powered support under bumping load. *J. Coal Sci. Technol.* **40** (12), 66–70 (2012).
21. Zhang, J. Z. & Zhang, J. L. A study on liquid shock of energy-absorbing anti-impact hydraulic column. *J. Vib. Shock.* **39** (08), 51–57 (2020).
22. Pan, Y. S., Xiao, Y. H., Li, Z. H. & Wang, K. X. Study of tunnel support theory of rockburst in coal mine and its application. *J. China Coal Soc.* **39** (02), 222–228 (2014).
23. An, D. et al. Study on improvement of prefolded energy absorption device to constant resistance and its mechanical properties. *J Sci. Progr.* **104**(3), (2021).
24. Xu, H. L., Guo, X., Song, Y. M. & An, D. Analysis on characteristics of anti-impact and energy absorption of new type of composite folding column used in mining. *J. Coal Sci. Technol.* **51** (03), 225–232 (2023).
25. Tian, L. Y., Zhou, Y. P., Sun, Y. X. & Yu, L. Energy absorption performance of multicellular thin-walled energy-absorbing components of anti-shock support columns. *J. China Coal Soc.* **48** (05), 2224–2235 (2023).
26. Du, M. C. et al. Comparison and analysis of energy absorption characteristics of chiral structure in novel energy buffering absorption device. *J. Coal Sci. Technol.* **51** (S1), 396–403 (2023).

Acknowledgements

Author contributions

D.A. and J.F. completed the main text of the paper, and Y.S. checked the content, L.X. The illustrations were sorted out, and all the authors participated in the experimental and simulation data processing.

Declarations

Competing interests

The authors declare no competing interests.

Additional information

Correspondence and requests for materials should be addressed to H.X.

Reprints and permissions information is available at www.nature.com/reprints.

Publisher's note Springer Nature remains neutral with regard to jurisdictional claims in published maps and institutional affiliations.